

Article

Modelling Recent and Future Climate Scenarios Impact on Malaria Transmission in Senegal Using Bias-Corrected CMIP6

Ibrahima Diouf^{1,*}, Jacques-André Ndione², Amadou Thieno Gaye³

¹ Laboratoire de Physique de l'Atmosphère et de l'Océan-Siméon Fongang, Ecole Supérieure Polytechnique de l'Université Cheikh Anta Diop (UCAD), BP 5085, Dakar-Fann, Dakar 10700, Senegal; ibrahima23.diouf@ucad.edu.sn (I.D); atgaye@ucad.edu.sn (A.T.G)

² Regional Agency for Agriculture and Food) 83 Rue des Patures (Super Taco), 01 BP 4817 - Lomé, Togo; jac-andrendione@yahoo.fr (J.A.N)

* Correspondence: ibrahima23.diouf@ucad.edu.sn; Tel.: +221 78 381 69 87

Abstract: Malaria is a constant reminder of the climate change impacts on health. Many studies have investigated the influence of climatic parameters on the of malaria transmission. Climate conditions can modulate malaria transmission through increased temperature, which reduces the duration of the parasite's reproductive cycle inside the mosquito. The intensity and frequency of the rainfall modulate the development of the mosquito population. In this study, the Liverpool Malaria Model (LMM) is used to simulate the spatio-temporal variation of the malaria incidence in Senegal. The simulations are based on the WATCH Forcing Data applied to ERA-Interim data (WFDEI) used as a point of reference, and biased-corrected CMIP6 models, separating historical and projections for 3 Shared Socio-economic Pathways scenarios (SSP126, SSP245 and SSP585). Our results highlight a strong increase in temperatures, especially towards eastern Senegal under the SSP245 but mainly the SSP585 scenarios. The ability of the LMM model to simulate the seasonality of malaria incidence is assessed. The model reveals a period of high malaria transmission between September and November with a maximum reached in October. Results indicate a decrease in malaria incidence in certain regions of the country for the far future and for the extreme scenario. This study is importance for the planning, prioritization, and implementation of control activities in Senegal.

Keywords: projections; CMIP6; climate; impacts; health; malaria; Malaria; Senegal.

1. Introduction

The threat of climate change is well known, and it has a huge impact on the emergence and re-emergence of certain vector-borne infectious diseases such as malaria. This disease is continuing to evolve in a changing world and so do their geographical distributions due to vectors transmission which is influenced by the temperature raise, moisture availability, rainfall, and drought periods. The health impacts of climate change will not be evenly distributed [1], and the distribution of the most severe health burdens is almost opposite to the global distribution of greenhouse gas emissions. The Intergovernmental Panel on Climate Change (IPCC) has concluded that to avert catastrophic health impacts and avert millions upon millions of climate change-related deaths, the world must avoid or even limit the increase temperature at 1.5°C [2–4]. Past emissions have already caused some temperature rise and other inevitable changes. Global warming, even of 1.5°C, is not to be considered insignificant because every tenth of a degree of additional warming will have impacts on the lives and health of populations [5]. Developing an effective and sustainable human health service, associated surveillance and emergency preparedness systems and sustainable disease control and prevention programs is perhaps the most important strategy for dealing with climate change The WHO Global Technical Strategy (GTS) for malaria sets a goal to reduce case incidence and malaria deaths by 90% by the

year 2030 referencing 2015 levels. These targets have been missed by 37% and 22% respectively because malaria-determining factors such as climate information, land use/cover change, resistance (parasite, insecticide, drug), accurate diagnosis, socioeconomic status, and other related environmental factors are not operationally used in African health decision-making processes. Malaria is now well documented by scientific work, not only on the clinic of diseases, but above all work related to variability and/or climate change. Studies exist occasionally on diarrhea diseases in relation to climate change but concern small spatial entities. Our study on this paper focuses on the evaluation of the past and current impact of seasonal and interannual climate variability on climate-sensitive diseases such as malaria over Senegal. Malaria is a vector-borne disease whose existence and transmission depend on three main factors: the plasmodium parasite, the Anopheles vector, and the human host. Beyond these essential factors, the risk of malaria transmission can be maintained or reinforced by environmental conditions, or climatic conditions as well as socio-economic factors. In particular, the transmission of malaria is very sensitive to climate and atmospheric conditions. When these are unusual, for example during heavy rainfall, mosquito populations can multiply and trigger epidemics. We had previously studied the climate-malaria relationship [6] as well as the predictability of high malaria occurrences in Senegal and West Africa in general [7]. With these studies, we have already noted a causal relationship between El Niño and malaria parameters. These results were endorsed in Diouf et al. [8] by coupling the LMM malaria model (Liverpool Malaria Model) of Hoshen et al. [9] and the SST-based statistical ForeCAST (S4CAST) of Suárez-Moreno and Rodríguez-Fonseca et al. [10].

This work is organized as follows: Section 2 presents the different types of data used and the methods applied. Section 3 studies the spatio-temporal variability of the health and climatic data (rainfall and temperature) over Senegal, and the malaria simulation variable with the LMM model forced by the various data presented previously. Finally, a summary and discussion of the main results are provided in Section 4.

2. Materials and Methods

2.1 Study area

Senegal is located at the westernmost tip of West Africa and lies within 1217°N latitude and 18-12°W longitude (Figure 1). Climate characteristics are very diverse across different ecoregions of West Africa, ranging from a Sahelian to a Sudano-Sahelian and a Sudano-Guinean climate. Toward the north of West Africa, including Senegal, the climate is Sahelian, with moderate rainfall occurring during a short rainy season (August-September). Senegalese climate is strongly modulated by the West African monsoon. Temperature in Senegal present a bimodal evolution with two peaks in May and October, on either side of the rains. The climate of Senegal is characterized by great spatio-temporal variability and its dynamics are generally dominated by a North-East wind regime (Harmattan) during the dry season and South-West during the rainy season (West African Monsoon). The period from December to February being the coldest, but the continental influence is more clearly visible in the east on the diurnal thermal difference. May and October are generally the hottest months for most of the country. The thermal differences are also found on the rainfall level. Rainfall decreases from south to north on the one hand and from west to east on the other. The first significant rains begin between June-July and are given by squall lines whose effectiveness decreases towards the West [11]. The rains continue until October. Cumulative rainfall varies from 300 mm to 1000 mm [12]. This description is based on the practices of African meteorologists who meet the Köppens classification [13].

Regarding climate change, like many Sahelian countries, Senegal faces many natural hazards such as floods, droughts, heat waves. The latter are extreme weather events generally characterized by the persistence of high temperature for several days. With the progression of climate change, these heat waves are expected to increase in number and intensity and everywhere in the world [14]. Events which, for some authors, are associated

with an increased risk of morbidity and mortality and therefore constitute a major public health threat.

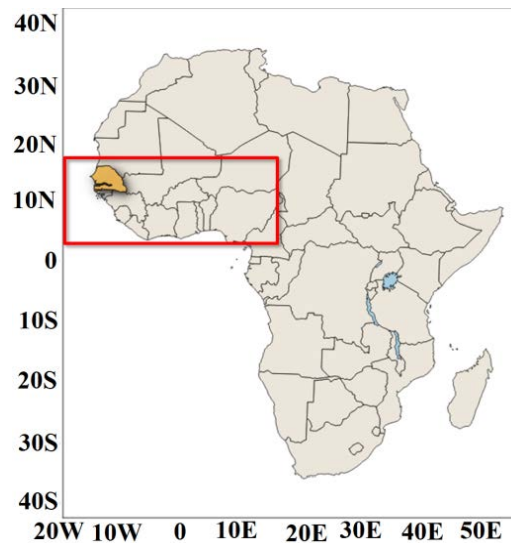


Figure 1. Location of the study area: Senegal [12N to 17N and 18W to 11W] is colored in yellow, located in West Africa [4N to 18N and 20W to 15E], which is delineated in red.

2.2 Data used

2.2.1 Malaria Data Surveillance

In terms of observation, we acquired malaria data from health districts, from MSAS sentinel sites. The health data obtained so far contains the number of cases of the disease recorded on an annual scale and by region. The clinical data correspond to the number of observed malaria cases obtained from the PNLP (Programme National de Lutte contre le Paludisme au Senegal; NMCP/National Malaria Control Programme in Senegal in English). The PNLP records malaria cases in the framework field surveys in Senegal. The observed numbers of malaria cases used in this study are collected from various health districts in Senegal for the period 2011-2021. These malaria data are recorded for all health districts and hospitals to derive a monthly time series for 14 administrative regions (Dakar, Diourbel, Fatick, Kafrine, Kaolack, Kedougou, Kolda, Louga, Matam, Saint-Louis, Sedhiou, Tambacounda, Thies, and Ziguinchor). These sentinel sites provide a good representation of malaria transmission in the different climatic zones of Senegal.

2.2.2 Climate data and methods

In this study, we have used climate data from the WATCH Forcing Data applied to ERA-Interim data (WFDEI) as reference data [15] and the multi-model ensemble mean of fifteen (15) global circulation models, for instance, Coupled Model Intercomparison Project, version 6, where bias correction technique, the CDF-t (Cumulative Distribution Function transform) method [16], was applied. The WATCH Forcing Data methodology applied to ERA-Interim data (WFDEI) [17], is produced from Watch Forcing Data (WFD) and ERA-Interim reanalyses via sequential interpolation at 0.5° resolution, an altitude correction and monthly scale adjustments based on monthly observational data from CRU (Climate Research Unit) TS3.1/TS3.21 and GPCCv5/v6. Details of the three products can be found in Dee et al. [15] for ERA-Interim and Weedon et al. [17] for WFDEI. The variables have a daily time step with a spatial resolution of 0.75° (~80 km) and 0.50° (~55 km) respectively for ERA-Interim and WFDEI, being qualified as low resolution and medium resolution.

Regarding the CMIP6, these simulations are available in daily time scale for the period 1850-2014 (Historical) and 2015-2100 (projections). The available models are shown in Table 2. They are available at different spatial resolutions (Table 1) which, for example,

ranges from 50 km (CNRM-CM6_HR) to more than ~300 km (CanESM5). The period 1985 to 2014 was chosen as the reference period.

Table 1. List of the global circulation models (GCMs) i.e., biased CMIP6 models used in the study

| Model name | Institution and country | Resolution |
|----------------------|--|-------------------|
| BCC-CSM2-MR | Beijing Climate Centre (BCC) and China Meteorological Administration (CMA), Chine | 1.1 x 1.1 |
| CanESM5 | Canadian Earth System Model, Canada | 2.81° × 2.81° |
| CESM2 | National Centre for Atmospheric Research, Climate and Global Dynamics Laboratory, USA | 1.25° × 0.94° |
| CMCC-CM2-SR5 | The Euro-Mediterranean Centre on Climate Change, Italie | 2.8° x 1.9° |
| CNRM-CM6_HR | Centre National de Recherches Météorologiques-Centre Européen de Recherches et de Formation Avancée en Calcul Scientifique, France | 0.5° x 0.5° |
| FGOALS-g3 | Flexible Global Ocean-Atmosphere-Land System model Grid-point version 3 | 2° x 2.3° |
| GFDL-ESM4 | Geophysical Fluid Dynamics Laboratory, SUA | 1.25° × 1.00° |
| IITM-ESM | Indian Institute of Tropical Meteorology, India | 1.9° x 1.9° |
| INM-CM5-0 | Numerical Mathematics, Russian Academy of Science, Moscow 119991, Russia | 2° x 1.5° |
| IPSL-CM6A-LR | Institut Pierre-Simon Laplace, France | 2.5° x 1.3° |
| MIROC6 | Japan Agency for Marine-Earth Science and Technology, Kanagawa 236-0001, Japan | 1.4° x 1.4° |
| MIROC-ES2L | Japan Agency for Marine-Earth Science and Technology, Kanagawa 236-0001, Japan | 2.8° x 2.8° |
| MPI-ESM1-2-HR | Max Planck Institute for Meteorology, High Resolution, Germany | 0.9° x 0.9° |
| NESM3 | Nanjing University of Information Science and Technology, Nanjing, | 1.9° x 1.9 |
| TaiESM | Research Centre for Environmental Changes, Taiwan | 1.3° x 1° |

To study possible future impacts, the IPCC (Intergovernmental Panel on Climate Change) in its 6th report [18] relies on five scenarios called Shared Socio-economic Pathways (SSP). Economists and sociologists assess the costs of adaptation and mitigation related to climate change according to different socio-economic scenarios compatible with the Representative Concentration Pathway (RCP) scenarios. The RCP are four trajectory scenarios of radiative forcing up to the year 2100. These scenarios were used in the IPCC Fifth Assessment Report (AR5). In the fifth assessment report of the IPCC (AR5, published in 2013) and based on four different hypotheses concerning the quantity of greenhouse gases that will be emitted in the years to come (period 2000-2100), each scenario RCP gives a variant deemed probable of the climate which will result from the level of emission chosen as working hypothesis. The four scenarios are named after the range of radiative forcing thus obtained for the year 2100: the RCP 2.6 scenario corresponds to a forcing of +2.6 W/m² (Watt per square meter), the RCP 4.5 scenario to + 4.5 W/m², and the same for the

RCP6 and RCP8.5 scenarios. The latest scenarios, so-called SSPs, are presented according to the efforts that will need to be made in terms of adaptation and mitigation if the world is moving towards such scenarios.

The LMM model is forced by daily rainfall and daily temperature data from the WFDEI, and the multi-model ensemble mean of the bias-corrected CMIP6 data to develop malaria incidence in different climatological periods, using historical experiments and SSP126, SSP245 and SSP585 emission scenarios separately. The datasets (observed and simulated) used were interpolated on the same grid to make them consistent. The LMM takes climate data at this interpolated resolution. The bias-corrected CMIP6 data used in this work were obtained from the LMDZ server (LMD stands for the Laboratoire de Météorologie Dynamique, the "Z" in LMDZ stands for "zoom" and refer to the regional refinement capacity of the grid). The data process was performed using a MATLAB language that includes several functions for mapping NetCDF data and organizing time series to be easily used within the box plot function.

The Taylor diagram described by Taylor et al. [19] is used to evaluate the performance of CMIP6 (multi-model ensemble) models against the WFDEI data used as a point of reference. This diagram offers the advantage of representing at the same time 3 statistics which are the mean squared error (RMSE for Root Mean Square Error in English), the standard deviation of the simulation compared to the observation (or reference data) and the correlation coefficient between observation and simulation. It was invented by researcher Karl E. Taylor in 1994 and is frequently used by meteorologists and atmospheric scientists. The most used statistic to quantify the similarity between observed and simulated values is the correlation coefficient. This coefficient makes it possible to detect the presence or absence of a linear relationship between two continuous quantitative characters. The correlation coefficient measures the degree of connection or dependence between two quantitative traits. It is between -1 and 1. The best method is the one that maximizes the correlation coefficient. Standard deviation is the most used measure of data dispersion in statistics. The lower the standard deviation, the less the values are dispersed around their mean. The root mean square error is the square root of the arithmetic mean of the square of the difference between the observed and simulated values. The calculation of the RMSE provides us with information on the amplitude of the deviations. The best method is the one that minimizes the RMSE. The RMSE is an appropriate error measure for data that exhibits very high seasonality. The correlation coefficient and the root mean square error provide additional statistical information to quantify the correspondence between two sets of data, for a more complete characterization of the observed and estimated data.

2.3 LMM malaria model

The LMM (Liverpool Malaria Model) is a dynamic model of malaria based on daily time series of rainfall and temperature. The different components of the malaria transmission model and the calibration of the parameters are described in more detail by Hoshen and Morse [9] then Ermert et al. [20]. The LMM is a mathematical-biological model of parasite dynamics, which includes intra-vector phase dependent on meteorological conditions and phase within the host independent of meteorological conditions. The mosquito population is simulated using larval and adult stages, the number of eggs deposited in the breeding sites and the larval mortality rate according to the rains of the previous 10 days. The mortality rate of adult mosquitoes and the egg-laying/biting cycle (called the gonotrophic cycle) depend on temperature. The process of parasite transmission between humans and mosquitoes is modelled with a temperature dependence for the parasite reproduction rate (sporogonic cycle) and mosquito biting rate. The two cycles evolve according to the number of "degree-days" above a certain temperature threshold. Respectively, gonotrophic and sporogonic cycles take about 37 degree-days and 111 37 degree-days with a threshold of 9 C (18 C) [21]. Climate and health studies have used LMM simulations in southern Africa, including Zimbabwe, Botswana and across the African continent [22] and [23][23]. The output variables of the model are, among others, the incidence,

prevalence, mosquito population, etc. The current version of the model (LMM2010) has shown significant improvements in the simulation of malaria dynamics in sub-Saharan African countries including Senegal.

3. Results and Discussion

3.1 CMP6 models' evaluation: validation of the rainfall and temperature inputs

Figure 2a shows the distribution of normalized rainfall anomalies for each year of the validation period by comparing historical time series with WFDEI data (observations). The boxplot highlights the minimum, maximum, median, and average values of rainfall averaged over Senegal over the climatological period from 1985 to 2013 respectively of WFDEI and CMIP6 (historical). The years when the CMIP6 rainfall median is positive (negative) largely correspond to the years when the WFDEI is also positive (negative). In Figure 2b, if we make the projection on the axis of the correlations, we note that the correlation coefficient is around 0.95, and for the mean squared error, considering the semicircles whose origin is centered around 1, we see that the red point is between 0 and 0.25, so approximately, the root mean square error is 0.1. For the standard deviation, considering the semicircles whose origin is centered around 0, we see that the red point is between 0.75 and 1, so the corresponding value is approximately 0.8.

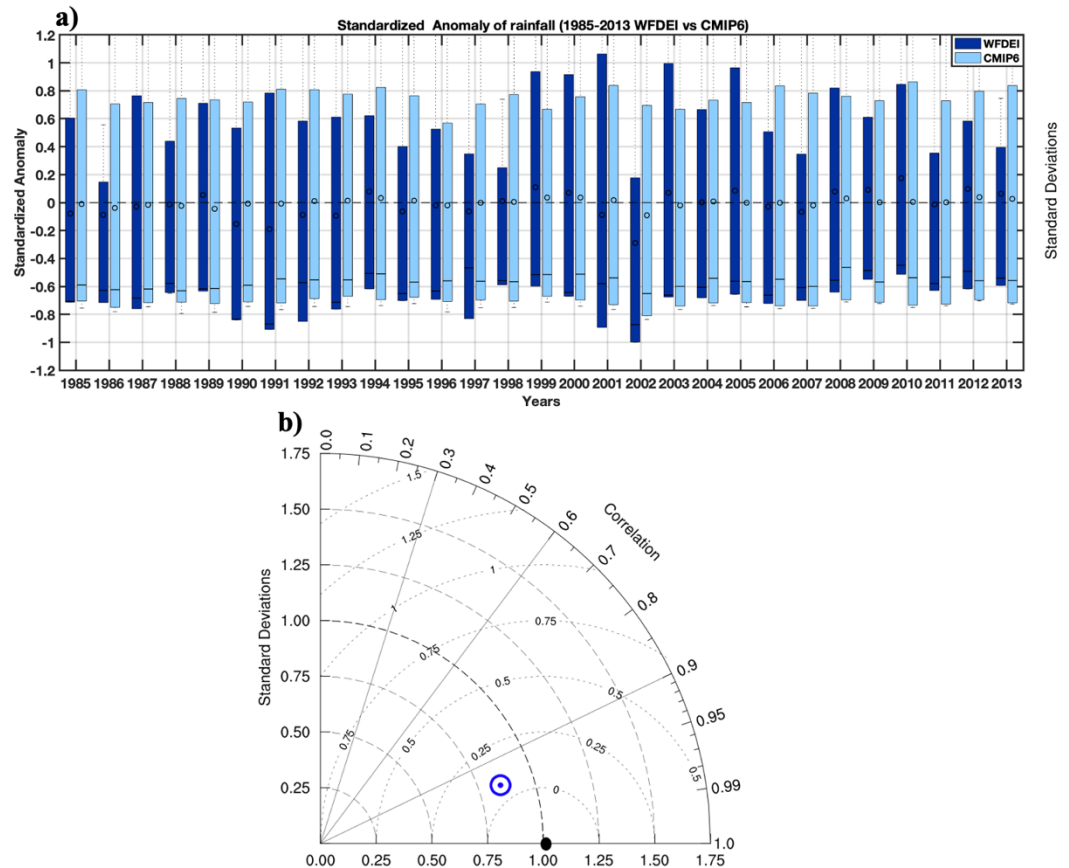


Figure 2. a) Standardized temperature anomalies for each year of the validation period (1983-2013) for WFDEI and CMIP6. b) Normalized Taylor diagram displaying the statistics (coefficients, standard deviations and mean square errors) of rainfall comparing multi-model ensemble mean of the bias-corrected CMIP6 with reference climate data (WFDEI). The multi-model ensemble mean of the bias-corrected CMIP6 compared is shown by the blue cycle and the WFDEI used as a point of reference is shown by the black dot point on the x-axis.

Figure 3a shows the distribution of normalized temperature anomalies for each year of the validation period by comparing historical time series with WFDEI data (observations). The years when the CMIP6 temperature median is positive (negative) largely correspond to the years when that of the WFDEI is also positive (negative) with some exceptions such as for the years 1989 and 1999. In Figure 3b, we note that the correlation coefficient is around 0.93, and for the mean squared error, considering the semicircles whose origin is centered around 1, we see that the red point is between 0 and 0.25, so approximately 0.23. For the standard deviation, considering the semicircles whose origin is centered around 0, the corresponding value is exactly 0.75.

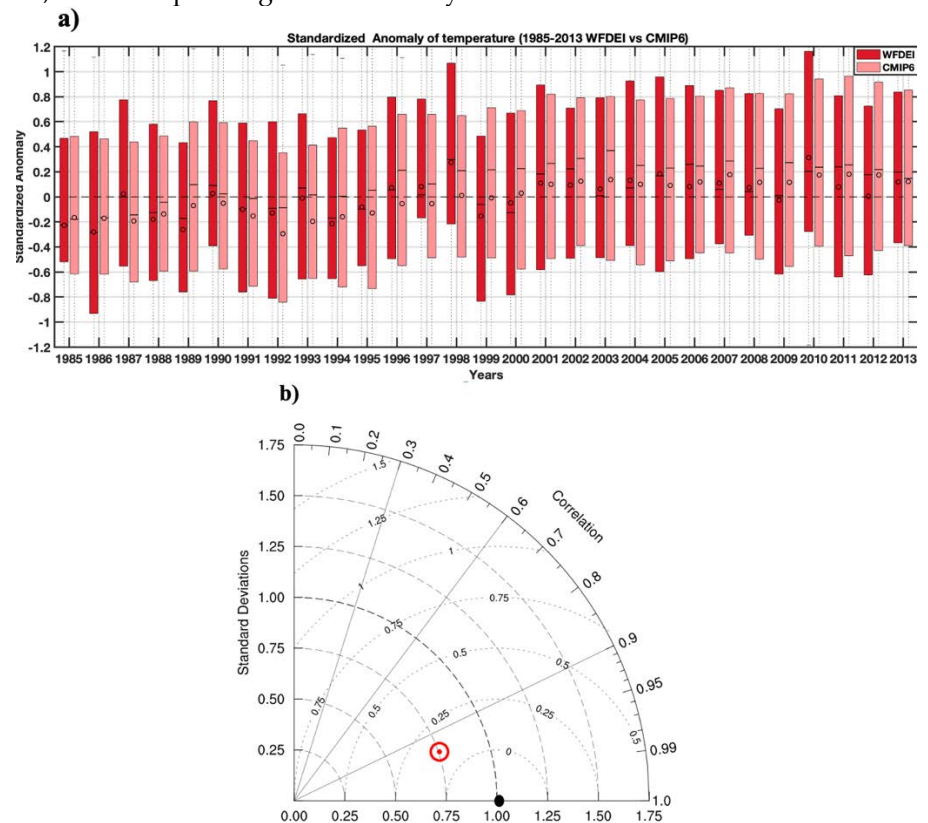


Figure 3. Same as in Figure 2 but for temperature

3.2 Projected changes in the spatio-temporal variability of the CMIP6 data

3.2.1 Projected changes in the spatio-temporal variability of the CMIP6 rainfall

In Figure 4, the spatial distribution of rainfall variables is represented for the historical period (1950-2014), under the SSP126, SSP245 and SSP585 scenarios for the 2015-2080 projection period (common period of the different models used for the ensemble mean). A latitudinal gradient is observed on the rainfall maps. These results also show a decrease in rainfall for the projections. The particular interest aroused by Figure 5a is explained by the fact that it reveals the largest rainfall deficit ever recorded during the 20th century in Senegal. The marked drought of the 1970s is the most serious event recorded in the historical period. The multi-decadal variability shows an alternation of wet and dry periods. Between two wet periods (1950-1970 and 2005-2010) there is a period of intense drought. The curve representative of the multi-decadal variability shows that during the wet period (the years 1950' and 1960'), we observe dry sequences (in 1957, 1960 and 1965 and 1966). Thus, we observe the year 1977 relatively wet during the period of great drought of the 1970s.

In Figure 5b, the variation in the amplitude of rainfall is much more marked between the months of July and August, with the SSP585 scenario. On the other hand, the rainfall regime almost maintained between the historical and the SSP126 and SSP245 scenarios

with a peak of 200 mm in August. The different time series are consistent with the annual cycle characterized by a single rainy season in the year (from May to October) with maximum rainfall in August. Figure 5c represents the interannual variations in rainfall for the historical periods and scenarios SSP125, SSP245 and SSP585. The significant difference between the historical dataset and the three scenarios is noted on the interannual variability (Figure 5c). The comparison on the interannual variability reveals a clear decrease in rainfall for the projections, with the extreme scenario SSP585, but also with the scenarios sSSP126 and SSP245 to a lesser extent.

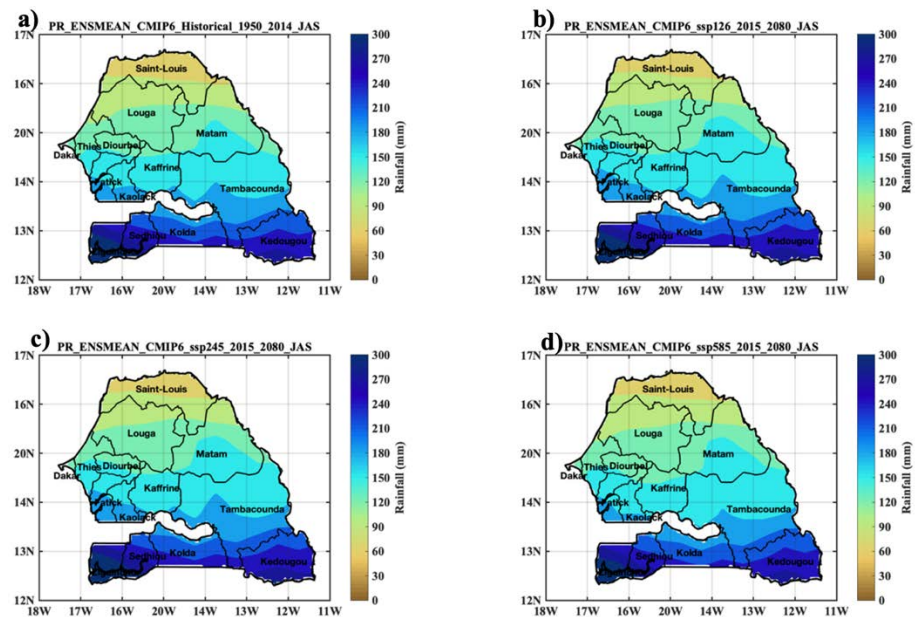


Figure 4. Spatial distribution of rainfall in Senegal in June-August-September with historical data (1950-2014), and projections (2015-2080) for the scenarios SSP12.6, SSP245, SSP585 of the CMIP6 ensemble models.

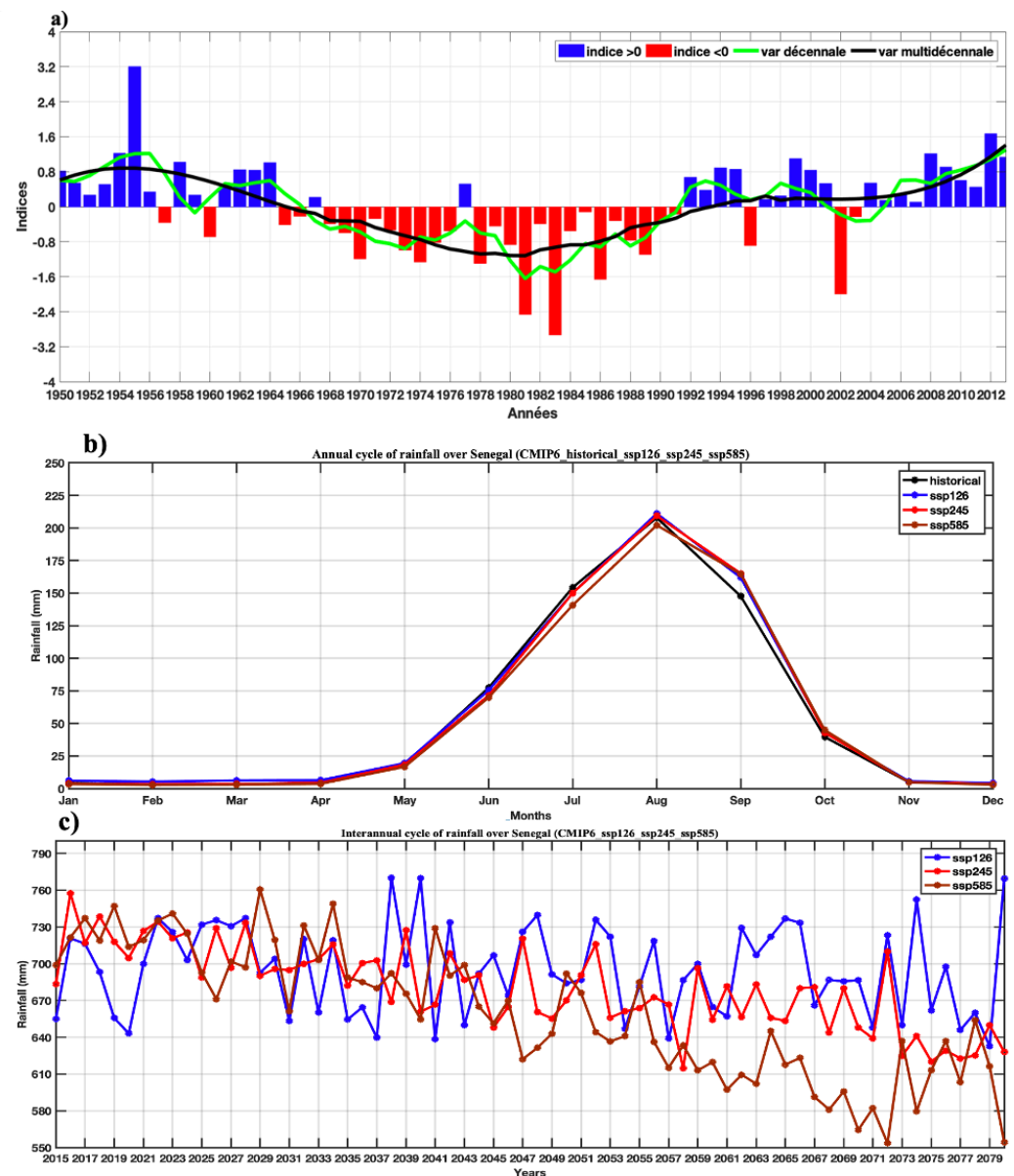


Figure 5. a) Trend of average rainfall over Senegal for the historical period 1950-2013 (Overall average of CMIP6 models) highlighting interannual variability, decadal and multi-decadal variability, a) and b) respectively annual cycle and interannual variability rainfall in Senegal with historical data (1950-2014), and projections (2015-2080) for the SSP126, SSP245, SSP585 scenarios of the CMIP.

3.2.2 Projected changes in the spatio-temporal variability of the CMIP6 temperature

Figure 6 clearly highlights global warming with an increase in the signal in the projections compared to the historical period. The highest temperature generally prevails in the interior of the country but also in the eastern part of Senegal both for historical and for projections datasets. The lowest temperature values occur over portions of Senegal coastal area. The scenarios SSP245 and SSP585 indicate a sharp increase in temperature for the future, particularly towards eastern parts of Senegal, with monthly average temperature ranges approaching 32 °C to 33 °C for the SSP245 and 32C for the SSP585. Figure 7 represents the evolution of the average temperature over Senegal for the historical period 1950-2013, and the average annual cycles of three time series, namely the historical, and the projections under SSP126, SSP25 and SSP585 scenarios. During the historical period, the upward trend in temperature is better appreciated considering the decadal evolution (Figure 7a). The increase is clearly perceptible over the year-to-year variability, even if the

period 1950-1990 is marked by negative standardized anomalies (Figure 7a). The annual regime (Figure 7b) of the temperature with the different time series shows an increase for the projection period and this, with all 3 scenarios considered. The annual cycle indicates a bimodal temperature cycle, one in May and the other in October. The analysis of the monthly temperature evolution indicates that the hottest months are March, April, May, June, October, and November with a temperature above 30°C. On the other hand, the temperature is relatively low in August and September with values between 28 and 30°C due to the influence of cloud cover and heavy rainfall during the rainy season. Temperature remains relatively high during the year. Indeed, the climate conditions during the year in Senegal can be categorized into different seasons:

- between December and January, there is a period marked by a dry climate and very low temperature linked to the polar invasions during the winter season.
- between February and May, it is very hot and dry with the first peak in temperature in May, this absolute peak in temperature precedes the start of the rainy season;
- the period from July to September (rainy season) is very rainy wet with mild temperature due to cloud cover;
- the last period of this classification extends between October and November and is marked by high humidity and slightly high temperature. The second peak of the annual temperature cycle is often occurring in October with a peak approaching 32 °C.

For interannual the variability (Figure 7c), significant changes in temperature are clearly exhibited. We can see a regular trend reflected in rising temperature since the beginning of the projection period (2015). Moreover, we even see this tendency of increased temperature since the historical period, which is getting worse in the projections.

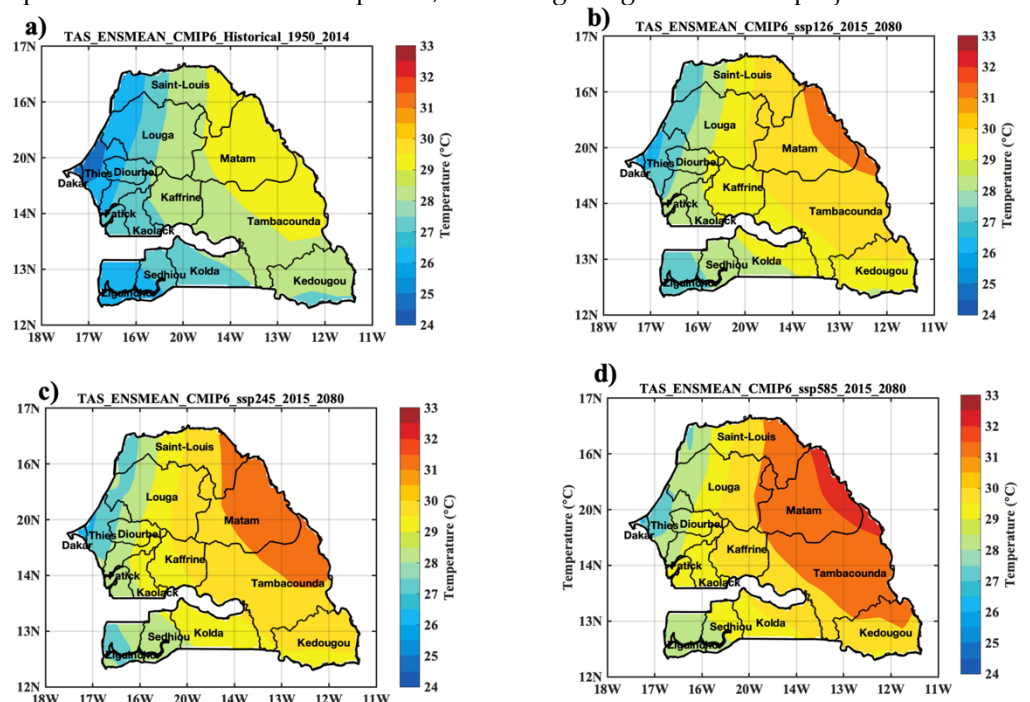


Figure 6. Same as in Figure 4, bur for temperature

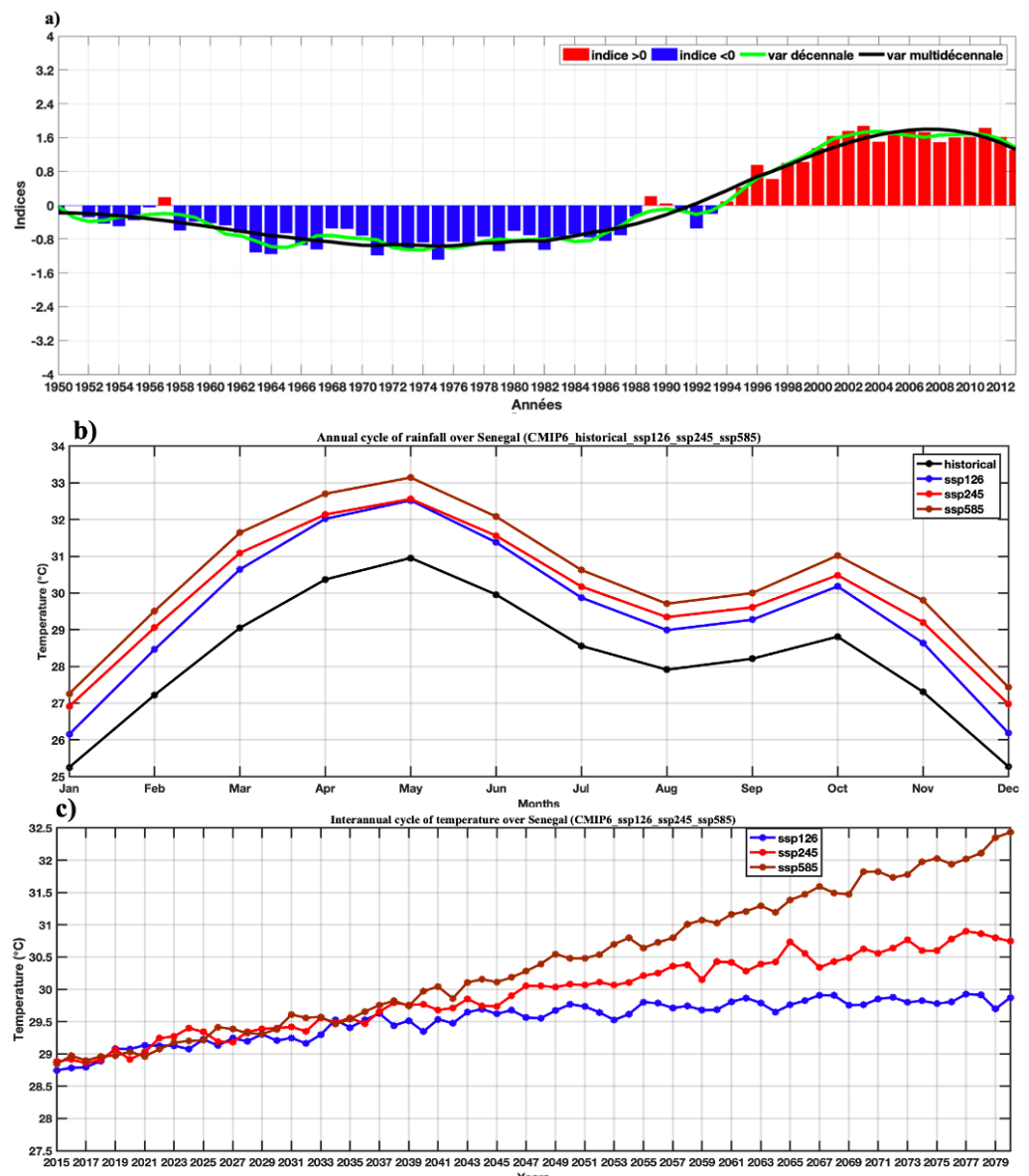


Figure 7. Same as in Figure 5, but for temperature.

3.3 Simulated malaria incidence in Senegal

In Figure 8, we analyze the spatio-temporal variability of malaria incidence simulated by the LMM model forced by daily rainfall and temperature data of the reference data (WFDEI). In There is a clear difference in the intensity of the malaria incidence signal between the northern and southern regions of Senegal. A very intense signal is observed in the southern part of Senegal, while in the far north, the signal is very weak. Indeed, the strong occurrence only extends around 15 °N. Malaria transmission prevails over the country notably between 11 °N and 15 °N. A particularly high signal is observed during the September-October-November season with a maximum in October.

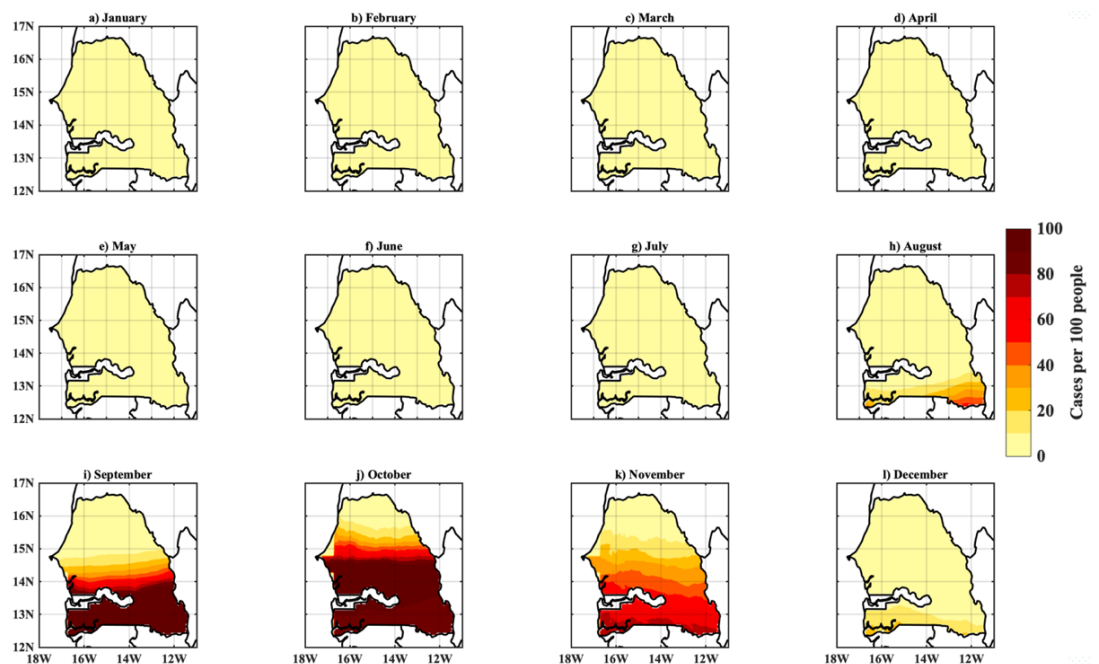


Figure 8. Spatial distribution and seasonal evolution of malaria incidence for the period 1979-2018: LMM model simulations based on WFDEI data.

The annual cycle of the simulated malaria incidence is shown in Figure 9. The analysis of the seasonal evolution shows an incidence rate close to zero during the period from January to June. From July, we see an increase in malaria incidence which peaks in October approaching 70%. Malaria transmission follows the rainfall regime. The rainy season is the period of high mosquito density. Other studies have shown that the peak of malaria mostly follows the peak of rainfall. Thus, the season of high malaria transmission has a maximum shifted by one to two months compared to the rainfall. The lag between the peaks of rainfall and the malaria incidence is explained by the fact that intermittent rains (or showers) in August can on the one hand strengthen the development of the population mosquito vectors triggered at the onset of the first rains, but these heavy rains in August mainly flush the female mosquitoes' eggs deposited on water surface. In addition, the mild temperature implied by the succession of rainy days are unfavorable for the mosquitoes' development, from larvae to infectious mature mosquitoes through the nymph stage. On the other hand, with a delay of 1 to 2 months, the mosquito vectors have their living conditions improved with the wastewater, warm and humid conditions (humidity increases the longevity of mosquitoes), environmental conditions including availability of ponds and vegetation cover. This delay is quite logical in relation to what is known about the biology of the *Anopheles* vector and the sporogonic cycle of the plasmodium parasite.

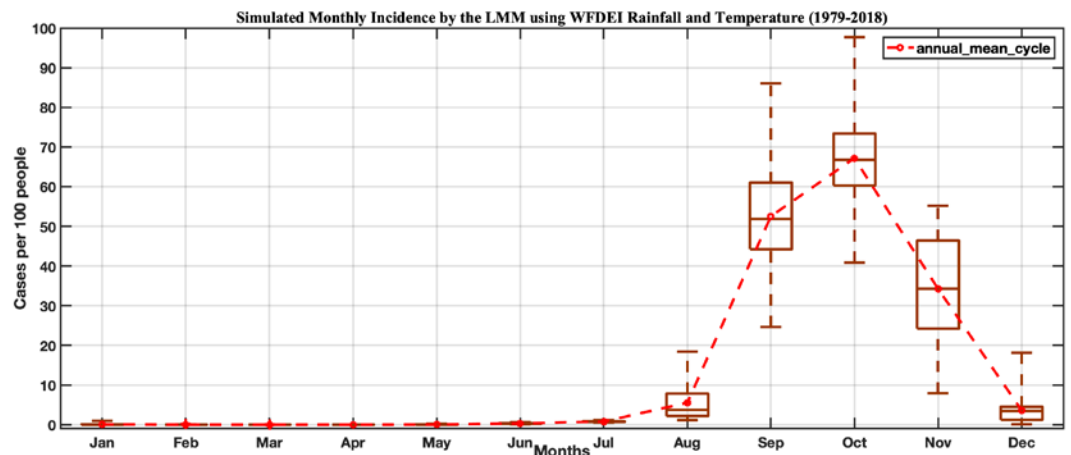


Figure 9. Intra-annual variation in incidence for the period 1979-2018: LMM model simulations based on WFDEI data.

Figure 10 shows the latitudinal incidence gradient, highlighting the difference between the north and the South. We see that the malaria incidence decreases from the latitude 12°N towards the high latitudes 16°N . In general, the parameters of malaria increase from North to South. So, they follow the latitudinal gradient of rainfall in Senegal but also the environmental conditions.

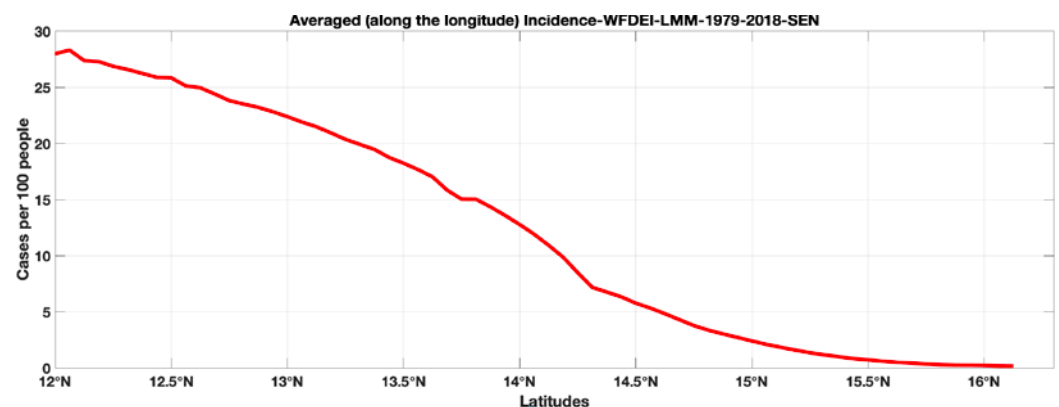


Figure 10. Latitudinal variation in incidence for the period 1979-2018: LMM model simulations based on WFDEI data.

The Hovmöller diagram (Figure 11) of malaria incidence indicates again that the maximum is observed in September-October. The high malaria transmission season occurs from September to November. High malaria incidence prevails throughout the area with an unequal distribution, the most affected regions are in the south (below 14.5°N) compared to the North (above 14.5°N). This difference between the north and the south is also implied by significant vegetation cover and optimal temperatures for the malaria transmission. The Hovmöller diagram also indicates the year-to-year variability of the malaria incidence. Figure 12 shows an average intensity of the malaria incidence from 1985 to 2014. The signal is relatively strong between 2000 and 2010.

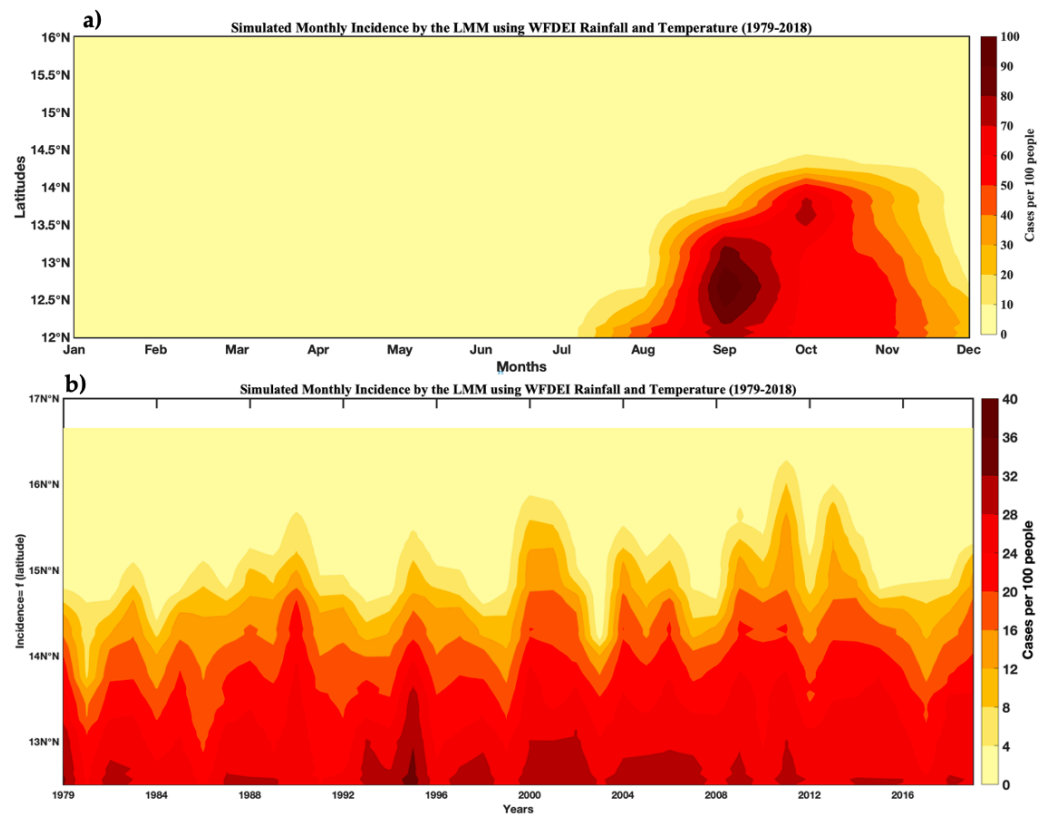


Figure 11. Hovmöller diagram of malaria incidence for the period 1979–2018: LMM model simulations based on WFDEI data: a) annual variability and b) Interannual variability.

3.4 validation of simulated malaria incidence in Senegal

In Figure 12a, the mean annual values of malaria cases, malaria incidence and climatic data (rainfall and temperature) have been represented. The high malaria transmission period extends to three months in observation and simulation. For the observed malaria cases, the period September–October–November is marked by an increased occurrence of malaria, with the maximum intensity of signal prevailing in October. For the malaria incidence also, the substantial transmission period is August–September–October with a maximum in October. The model performs well in the simulations of the high malaria transmission period. The interannual variability of the climatic and malaria parameters are shown in Figure 12b. The model well reproduced the interannual variability of transmission. Low malaria in 2002 was implied by particularly dryness in Senegal during this year. In general, corresponding years of positive (negative) malaria case anomalies and malaria incidence anomalies during positive (negative) rainfall anomalies are observed. In 2010, 2012, and 2015, high malaria transmission was observed in both observed malaria cases and the simulated malaria incidence. A decrease in malaria prevailed in the latest year of the time series. Figure 12b shows that temperature plays a role in the annual variability of malaria. On the other hand, the role that rainfall plays in the transmission of malaria is predominant for a variation from one year to another. It is also important to note that the warm temperatures can impact the adult mosquito survival scheme by starting to kill lots of adult mosquitoes in the model, which can imply a decrease in malaria transmission. In Figure 12c et 12d, a marked interannual variability of malaria is indicated and the simulated seasonality of malaria over Senegal is well-represented. A clear corresponding signal with high intensity is found in the observed malaria cases and simulated malaria incidence.

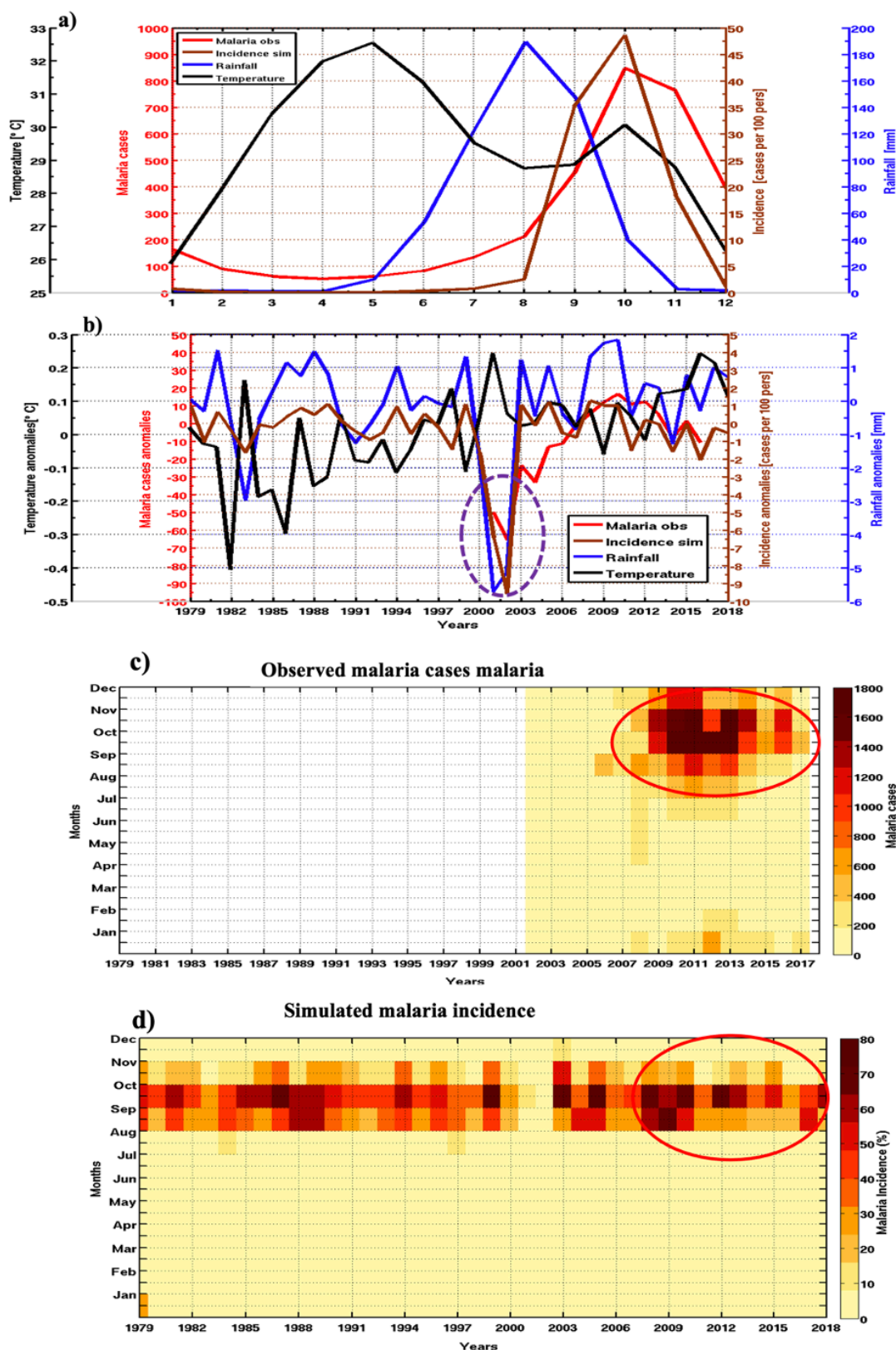


Figure 12. Comparison of the intra- and interannual variability of temperature, rainfall, observed malaria cases, and simulated malaria incidence in Senegal from 2002-2017: a) annual cycle of and b) interannual variability; c) et d) Intra- and interannual variability of malaria cases and simulated malaria incidence in Senegal from 2001–2017

3.5 Projected changes in the malaria incidence based on CMIP6 data

Figures 13a and 13b illustrate consistency between the malaria incidence simulated by the LMM model forced by the WFDEI (reference data) and that obtained from the CMIP6 data, both with the historical and with the different scenarios. For the spatial variability, there is still a clear difference in the intensity of the signal of the malaria incidence between the northern regions and the southern of Senegal. The latitudinal gradient of the distribution of malaria in Senegal would be still maintained. By comparing with historical data (Figures 13a and 13b), we find that the simulated malaria incidence decrease likely tends to prevail over many portions of Senegal, in the north and the centre, and this, even in the near future (2015- 2044), but especially in the far future (2050-2080), with the magnitude of the decrease greater with the SSP245 and SSP585 scenarios (Figure 13d, 13e, 13g et 14h). Such a decrease in malaria in the far future appears to be associated with climate change [24], [25] and [26]. Thus, temperatures that are too hot could have a negative impact on the adult mosquitoes' survival by starting to reduce the population of adult mosquitoes in the model and this implies a decrease in malaria transmission. Béguin et al. [23] showed an opposite effect of climate change on the global distribution of malaria, and they show a decrease in simulated malaria behaviors over the Sahel regardless of the period and scenario considered which are related to temperature effect. However, looking at the southern part of Senegal in Figures 13c and 14f and comparing with Figure 13a as a point of reference, malaria is expected to increase in the southern part of the study area. This agrees with the results of previous studies on West Africa such as Peterson [27] showed that the epidemic fringe would be shifted to the south for most of malaria models. It is expected that during the 2080s, the climate will become so unsuitable in the northern part of the Sahel including the northern regions of Senegal, without more people at risk [28].

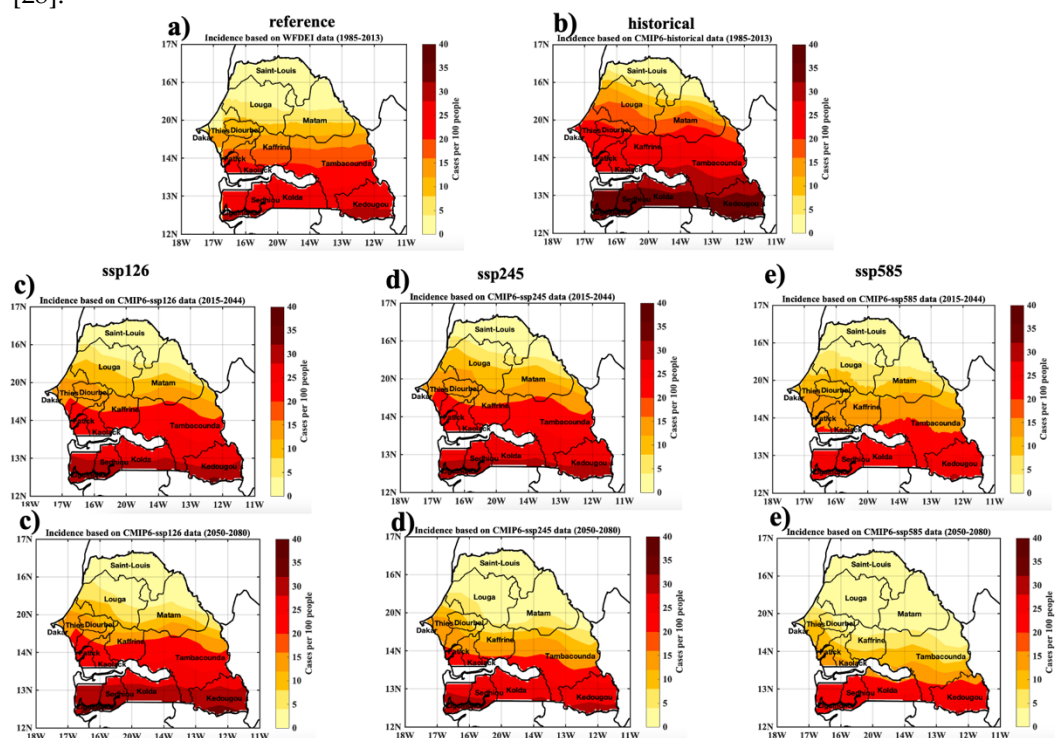


Figure 13. Comparison of the intra- and interannual variability of temperature, rainfall, observed malaria cases, and simulated malaria incidence in Senegal from 2002-2017: a) annual cycle of and b) interannual variability; c) et d) Intra- and interannual variability of malaria cases and simulated malaria incidence in Senegal from 2001-2017

Figure 14a illustrates the trend in the malaria incidence along the total historical used, i.e., period from 1950 to 2013. There is a drop particularly between the 1970s and the 1990s,

this decrease would be linked to the decline in rainfall during this period. On the annual cycle in Figure 14b, we observe that the transmission of malaria increases only between September and November with a peak in October, which is obtained with the climatology of the different time series. The projections in Figure 14c show more clearly the downward trend in the malaria incidence which would be linked to the drop in precipitation mentioned above, but also to temperatures that are too hot for the two scenarios SSP245 and SSP585. As for the SSP126 scenarios, it illustrates a slight increase in the malaria incidence in the far future.

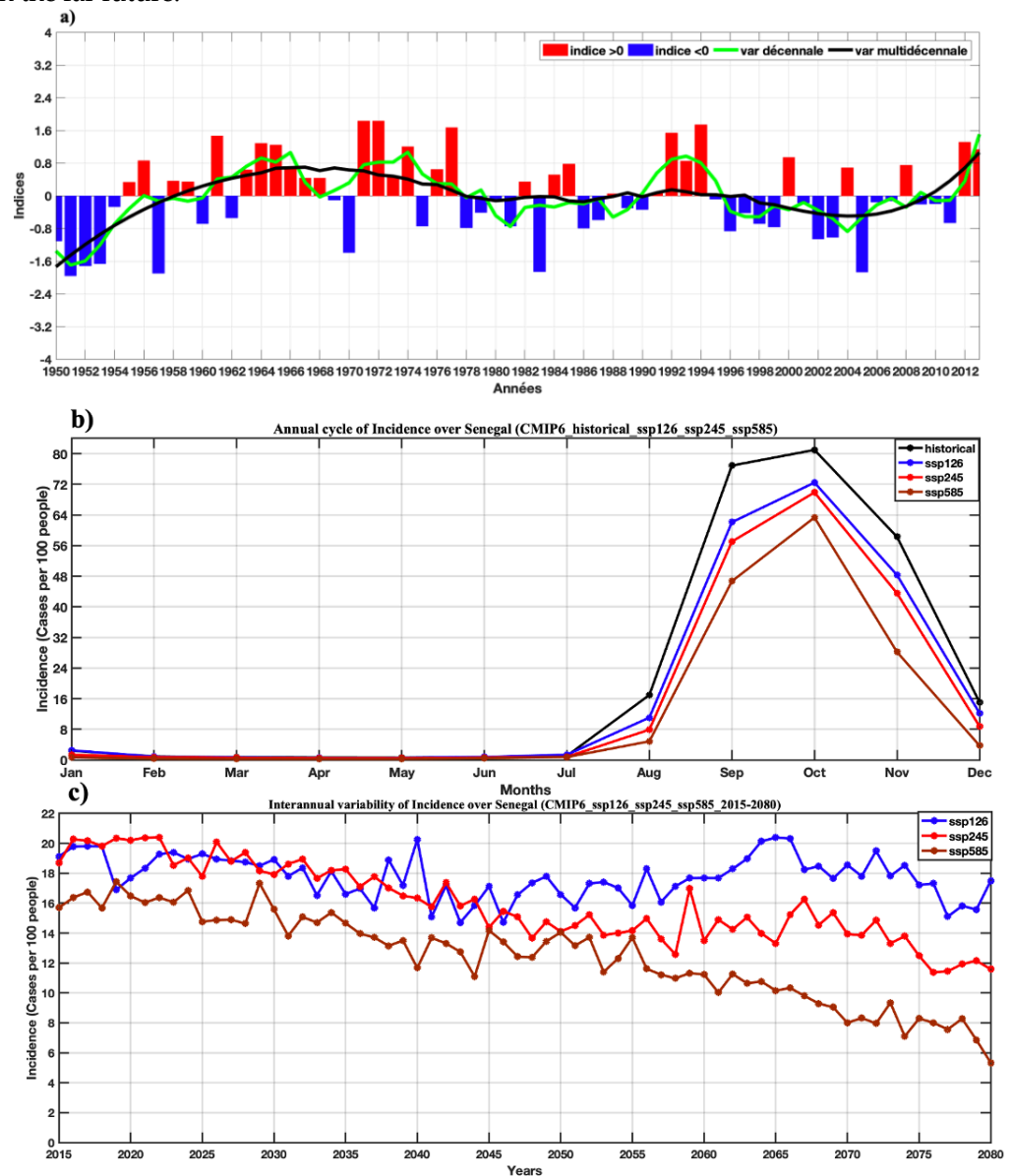


Figure 14. a) Trend in the malaria incidence averaged over Senegal for the historical period 1950-2013 (Simulation of the LMM model based on precipitation and temperature of the overall average of the CMIP6 models) highlighting the interannual variability, the variability decennial and multi-decadal: a) and b) respectively annual cycle of malaria incidence in Senegal with historical data (1950-2013), and projections (2015-2080) for scenarios SSP126, SSP245, SSP585 of CMIP6.

4. Conclusions

Climate projections for the Sahel, particularly in Senegal, include uncertainties for two reasons. On the one hand, because of the strong climate variability observed in the 20th century, it is more difficult to extract from the background noise a signal attributable to climate change; on the other hand, climate models give very divergent results for this

region. This divergence is particularly noticeable in the case of rainfall, where even the sign of the change is different between the models. For this reason, we consider here the multi-model ensemble mean of CMIP6 data from historical and the projections for rainfall and temperature. Given the wide divergence between models, it is always advisable not to base assessments of future climate change on the results of a single model, taken in isolation, so we work in study we work on an average of set of different models of CMIP6 (multi-model ensemble mean). The latitudinal gradient on precipitation in Senegal is well reproduced with CMIP6 data. There is a slight decrease in the precipitation signal in the projections. For the temperature, we note high temperature more localized in the east of the country but also inside the country to a lesser extent, both for history and for projections. The SSP245 and SSP585 scenarios showing a strong increase in temperatures for the future, especially towards eastern Senegal. Three statistical values including the mean squared error, the standard deviation, and the correlation coefficient indicate the performance of CMIP6 in reproducing rainfall and temperature observations (WFDEI).

The integration of LMM with future climate scenarios reveals effect of changes in rainfall and in temperature on changes in malaria transmission. Based on the findings of this study, malaria is expected to increase in the southern part of the study region in the future. This agrees with earlier findings in previous studies over West Africa which showed epidemic fringe shifted southward for most malaria models. Otherwise, it is expected that over the 2080s, the climate would become so unsuitable in the northern part of the Sahel, with no more additional people at risk. Some studies showed an opposing effect of climate change on the global distribution of malaria, and they show a decrease in the simulated malaria behaviors over the Sahel whatever period and scenario considered which is related to a temperature effect. The ability of the LMM model to simulate the seasonality of malaria incidence at the local scale is assessed. The model reveals a period of high malaria transmission between September and November with a maximum reached in October. This work is to ascertain how best to incorporate such a model effectively into a national decision-making process concerning health planning and interventions.

Author Contributions: Conceptualization, I.D., J.A.N. and A.T.G.; methodology, I.D.; validation, J.A.N. and A.T.G.; formal analysis, I.D. and J.A.N.; investigation, I.D. and J.A.N.; resources, J.A.N. and A.T.G.; writing—original draft preparation, I.D; writing—review and editing, I.D. and J.A.N.; supervision, A.T.G. and J.A.N.; project administration, A.T.G.; funding acquisition, I.D. and A.T.G. All authors have read and agreed to the published version of the manuscript.

Funding: This study is part of the Senegal National Adaptation Plan support Project - Global Environment Fund (NAP-GEF), Ministry of the Environment and Sustainable Development of Senegal. The authors present their warm thanks to the NAP-GEF who funded the study.

Institutional Review Board Statement: Not applicable.

Informed Consent Statement: Not applicable.

Data Availability Statement: All relevant data is presented within the manuscript. The WFDEI data are fully available without restriction, they are available from: <ftp://rfddata:forceDATA@ftp.iiasa.ac.at>. The bias-corrected CMIP6 data used in this work are available from the LMDz server, but the authors of this review do not have the right to openly make non-open access journal articles public.

Acknowledgments: We thank the University of Liverpool, where the LMM model was developed. We would also like to thank the Laboratoire de Physique de l'Atmosphère et de l'Océan-Siméon Fongang (LPAOSF) from which the authors of this work are affiliated. The authors would like to acknowledge the LMDz where CMIP6 simulations are extracted from.

Conflicts of Interest: The authors declare no conflict of interest. The funders had no role in the design of the study; in the collection, analyses, or interpretation of data; in the writing of the manuscript; or in the decision to publish the results.

References

1. A. Costello *et al.*, "Managing the health effects of climate change," *The Lancet*, vol. 373, no. 9676, pp. 1693–1733, May 2009, doi: 10.1016/S0140-6736(09)60935-1.
2. "IPCC | Global Warming of 1.5 °C, 2018 {Report} | Sustainability Resources | CFDA." <https://cfda.com/resources-tools/sustainability-resource-hub/sustainability-a-z-resources/detail/global-warming-of-1-5-oc-special-report#!> (accessed Aug. 04, 2022).
3. G. Cissé *et al.*, "Health, wellbeing, and the changing structure of communities," *Climate Change*, 2022.
4. C. C. IPCC, "Report of the intergovernmental panel on climate change," *IPCC report, Geneva, Switzerland*, 64p, 1995.
5. M. Romanello *et al.*, "The 2021 report of the Lancet Countdown on health and climate change: code red for a healthy future," *The Lancet*, vol. 398, no. 10311, pp. 1619–1662, Oct. 2021, doi: 10.1016/S0140-6736(21)01787-6.
6. I. Diouf *et al.*, "Comparison of malaria simulations driven by meteorological observations and reanalysis products in Senegal," *International journal of environmental research and public health*, vol. 14, no. 10, p. 1119, 2017.
7. I. Diouf *et al.*, "Climate Variability and Malaria over West Africa," *The American Journal of Tropical Medicine and Hygiene*, vol. 102, no. 5, pp. 1037–1047, May 2020, doi: 10.4269/ajtmh.19-0062.
8. I. Diouf *et al.*, "Oceanic Influence on Seasonal Malaria Incidence in West Africa," *Weather, Climate, and Society*, vol. 14, no. 1, pp. 287–302, Jan. 2022, doi: 10.1175/WCAS-D-20-0160.1.
9. M. B. Hoshen and A. P. Morse, "A weather-driven model of malaria transmission," *Malaria journal*, vol. 3, no. 1, pp. 1–14, 2004.
10. R. Suárez-Moreno and B. Rodríguez-Fonseca, "S<sup>4</sup></sup>CAST v2.0: sea surface temperature based statistical seasonal forecast model," *Geosci. Model Dev.*, vol. 8, no. 11, pp. 3639–3658, Nov. 2015, doi: 10.5194/gmd-8-3639-2015.
11. A. Gaye, "Caractéristiques dynamiques et pluviosité des lignes de grains en Afrique de l'ouest," PhD Thesis, PhD thesis, Université Cheikh Anta Diop, Dakar, Sénégal, 2002.
12. J. Le Borgne, "La pluviométrie au Sénégal et en Gambie, document multigraphié," *ORSTOM, Coopération française, Dakar*, 1988.
13. R. Cornforth *et al.*, "The First Forecasters' Handbook for West Africa," *Bulletin of the American Meteorological Society*, vol. 100, no. 11, pp. 2343–2351, 2019.
14. S. Russo, A. F. Marchese, J. Sillmann, and G. Immé, "When will unusual heat waves become normal in a warming Africa?," *Environmental Research Letters*, vol. 11, no. 5, p. 054016, 2016.
15. D. P. Dee *et al.*, "The ERA-Interim reanalysis: configuration and performance of the data assimilation system," *Q.J.R. Meteorol. Soc.*, vol. 137, no. 656, pp. 553–597, Apr. 2011, doi: 10.1002/qj.828.
16. P.-A. Michelangeli, M. Vrac, and H. Loukos, "Probabilistic downscaling approaches: Application to wind cumulative distribution functions," *Geophys. Res. Lett.*, vol. 36, no. 11, p. L11708, Jun. 2009, doi: 10.1029/2009GL038401.
17. G. P. Weedon, G. Balsamo, N. Bellouin, S. Gomes, M. J. Best, and P. Viterbo, "The WFDEI meteorological forcing data set: WATCH Forcing Data methodology applied to ERA-Interim reanalysis data," *Water Resources Research*, vol. 50, no. 9, pp. 7505–7514, 2014.
18. Z. Zhongming, L. Linong, Y. Xiaona, Z. Wangqiang, and L. Wei, "AR6 climate change 2021: The physical science basis," 2021.
19. K. E. Taylor, "Summarizing multiple aspects of model performance in a single diagram," *Journal of Geophysical Research: Atmospheres*, vol. 106, no. D7, pp. 7183–7192, 2001.
20. V. Ermert, A. H. Fink, A. E. Jones, and A. P. Morse, "Development of a new version of the Liverpool Malaria Model. II. Calibration and validation for West Africa," *Malar J*, vol. 10, no. 1, p. 62, Dec. 2011, doi: 10.1186/1475-2875-10-62.
21. C. Caminade *et al.*, "Mapping Rift Valley fever and malaria risk over West Africa using climatic indicators," *Atmosph. Sci. Lett.*, vol. 12, no. 1, pp. 96–103, Jan. 2011, doi: 10.1002/asl.296.

-
22. A. P. Morse, F. J. Doblas-Reyes, M. B. Hoshen, R. Hagedorn, and T. N. Palmer, "A forecast quality assessment of an end-to-end probabilistic multi-model seasonal forecast system using a malaria model," *Tellus A: Dynamic Meteorology and Oceanography*, vol. 57, no. 3, pp. 464–475, 2005.
 23. A. E. Jones and A. P. Morse, "Application and validation of a seasonal ensemble prediction system using a dynamic malaria model," *Journal of Climate*, vol. 23, no. 15, pp. 4202–4215, 2010.
 24. P. W. Gething, D. L. Smith, A. P. Patil, A. J. Tatem, R. W. Snow, and S. I. Hay, "Climate change and the global malaria recession," *Nature*, vol. 465, no. 7296, pp. 342–345, 2010.
 25. A. Béguin, S. Hales, J. Rocklöv, C. Åström, V. R. Louis, and R. Sauerborn, "The opposing effects of climate change and socio-economic development on the global distribution of malaria," *Global Environmental Change*, vol. 21, no. 4, pp. 1209–1214, Oct. 2011, doi: 10.1016/j.gloenvcha.2011.06.001.
 26. I. Diouf *et al.*, "Impact of future climate change on malaria in West Africa," *Theor Appl Climatol*, vol. 147, no. 3–4, pp. 853–865, Feb. 2022, doi: 10.1007/s00704-021-03807-6.
 27. A. T. Peterson, "Shifting suitability for malaria vectors across Africa with warming climates," *BMC infectious diseases*, vol. 9, no. 1, pp. 1–6, 2009.
 28. C. Caminade *et al.*, "Impact of climate change on global malaria distribution," *Proceedings of the National Academy of Sciences*, vol. 111, no. 9, pp. 3286–3291, 2014.